Scientific paper

Room-Temperature Synthesis and Optical Properties of $NdVO_4$ Nanoneedles

Mirela Dragomir[1,3,*] and Matjaž Valant[1,2]

[1] *Materials Research Laboratory, University of Nova Gorica, Slovenia*

[2] *University of Electronic Sciences and Technology of China, Institute of Fundamental and Frontier Science, North Jianshe Road No. 4 Section 2, Chengdu, China*

[3] *Present address: Department of Chemistry and Chemical Biology, McMaster University, Hamilton, Ontario, L8S 4M1, Canada*

* *Corresponding author: E-mail: mirela85.dragomir@gmail.com*

Received: 25-03-2018

Abstract

Tetragonal $NdVO_4$ nanoneedles were prepared via a simple room-temperature precipitation method in the absence of any surfactant or template, starting from simple inorganic salts, $NdCl_3$ and Na_3VO_4, as raw materials. The nanoneedles were characterized by XRPD, SEM, Raman, PL, and lifetime spectroscopy. The particles have a length of about 100 nm and a diameter of 20 nm and grow along <112> direction. The advantages of this method lie in the high yield, non-toxic solvents, mild reaction conditions, and that it can potentially be employed for the preparation of other 1D lanthanide vanadates.

Keywords: Nanostructures; Chemical synthesis; Optical properties; Raman spectroscopy; X-ray diffraction

1. Introduction

The interesting optical properties of lanthanides such as luminescence, up-conversion, wide optical transparency, or large birefringence originate primarily from the multitude of transitions within the $4f^n$ electronic states of the lanthanide ion. Thus, lanthanide-containing materials find applications as laser host matrices, optical polarizers, thermophosphors, sensors, solar cells, scintillators for γ-rays detection, in nuclear waste storage, ionic conductors, catalysts or photocatalysts.[1–5] The efficiency of the $4f^n$ excitations in a lanthanide ion can be enhanced through a charge transfer from a host material with a higher absorption coefficient. The orthovanadate group, VO_4^{3-}, is a good host for the trivalent ion because it can excite most of the lanthanide ions via the charge transfer transition within the VO_4^{3-} group, followed by an energy transfer to the emissive lanthanide ion. Choosing a crystal site with a very low symmetry for the lanthanide ion further increases the rate of absorption and emission, which can result in higher quantum yields.

In a tetragonal ABO_4 structure type, the A-site ion has a D_{4h} symmetry. Thus, a lanthanide ion sitting on this crystal site has a low symmetry which favours the electric dipole transitions resulting in higher radiative rate constants and less quenching processes. Neodymium vanadate, $NdVO_4$, is one of the most studied orthovanadate from the lanthanide orthovanadate family with the ABO_4-type structure. Numerous investigations have been made on optical materials based on $NdVO_4$ due to their good optical properties.[3,6,7] For example, Y-doped $NdVO_4$ is a well-known laser material with five times higher absorption coefficient at 808 nm (the standard wavelength of the currently available laser diodes) than the Nd:YAG laser diode.[6] The catalytic properties of $NdVO_4$ have also been investigated, i.e. for oxidative dehydrogenation of propane.[2] Additionally, it has been found that $NdVO_4$ exhibits a photocatalytic activity for degradation of dyes and organic pollutants comparable or even higher than that of the commercial TiO_2.[8,9] Another study indicated that Mo-doping increased the photocatalytic activity of $NdVO_4$ for the degradation of different dyes (e.g., methylene blue, rhodamine B, remazol brilliant blue).[4]

At ambient conditions, $NdVO_4$ adopts a zircon-type structure in the $I4_1/amd$ ($Z = 4$) space group with the lanthanide ion located in a polyhedron coordinated by eight oxygen ions. Under an applied pressure of about 6 GPa,

the zircon-type $NdVO_4$ undergoes a phase transformation to a metastable monazite-type structure with the space group $P2_1/n$ ($Z = 4$) where the Nd atoms are located in a eight-coordinate site (with eight unique Nd–O bond distances).[10,11] At around 11.4 GPa, $NdVO_4$ further transforms to a scheelite-type phase and so to a denser packing. All these phase transformations are accompanied by a decrease of the band gap by 0.5 eV (measured on a single crystal).[10]

Due to large specific surface areas and quantum size effects, nanocrystalline materials exhibit properties that are usually not observed in the bulk. Accordingly, the lanthanide orthovanadates in the form of nanocrystals show properties that make them potential multiphoton fluorescent materials, biochemical labels, solar cells, light emitting diodes (LEDs), oxidant sensors, and contrast agents in magnetic resonance imaging.[12–16] Therefore, the design and synthesis of the nanosized $NdVO_4$ opens up many opportunities for applications. Several methods have been developed for the synthesis of 0D, 1D or 2D $NdVO_4$ nanostructures such as: microwave synthesis, co-precipitation followed by thermal treatment, hydrothermal, metathesis reactions, or sonochemical synthesis.[8,17–21] Each of these methods has certain drawbacks – the requirement of either thermal treatment at high temperatures, long reaction time (up to several days), expensive equipment or the use of toxic solvents.

A new and simple method to obtain crystalline $NdVO_4$ nanoparticles at room temperature through a precipitation method, using a cheap and non-toxic solvent is reported in this study. In addition of being a very convenient and fast method, this route also conserves energy because it does not involve any thermal treatment.

2. Experimental Part

2. 1. Synthesis

The precipitation procedure for the synthesis of $NdVO_4$ nanoparticles employed in this study is summarized in the scheme depicted in Fig. 1.

In this method, $NdCl_3 \cdot 6H_2O$ (99.9%, Alfa Aesar) and Na_3VO_4 (99.9%, Alfa Aesar), were used as precursors and NH_3(aq) (25%) was the precipitating agent. Firstly, a $NdCl_3$ aqueous solution was prepared by adding 0.05 mol $NdCl_3 \cdot 6H_2O$ to 2 mL of distilled H_2O, while a Na_3VO_4 solution was prepared by dissolving 0.05 mol Na_3VO_4 in 3 mL of distilled H_2O. The pH of the final solution was adjusted to < 1 with a few mL of HCl(aq) (32%). Secondly, the two solutions were mixed slowly until a clear yellow solution resulted. NH_3(aq) (25%) was then added fast and under vigorous stirring to the above solution until the pH reached a value of ~11. A blueish-green precipitate formed. Then the obtained mixture was stirred for five more minutes before the precipitate was filtered, washed thoroughly with NH_3(aq) and then dried at room temperature overnight. The reaction that leads to the formation of $NdVO_4$ can be summarized as follows:

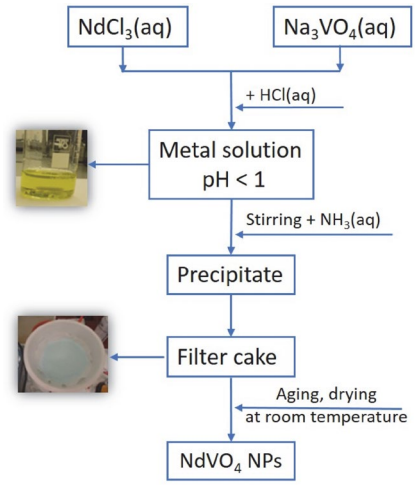

Fig. 1. A schematic representation of the synthetic procedure to obtain $NdVO_4$ nanoparticles.

$$NdCl_3(aq) + Na_3VO_4(aq) \xrightarrow{+NH_3(aq)} NdVO_4(s) + 3NaCl(aq) \quad (1)$$

2. 2. Characterisation

The phase composition was analysed by X-ray powder diffraction (XRPD) using a PANalytical X'Pert PRO diffractometer with Cu Kα_1 radiation (λ = 1.54056 Å). The X-ray powder diffraction pattern was collected over the 2θ range 5–80° with a step size of 0.017°. A structure refinement was conducted using *Topas* (version 6, Bruker, AXS, Karlsruhe, Germany). A fundamental parameters approach was used for the profile fitting.[22] A profile refinement was conducted in which the background (6th order Chebychev polynomial), the unit cell parameters, the scale factor, the crystallite size, the sample displacement, and preferred orientation were stepwise refined to obtain a calculated diffraction profile that best fit the experimental pattern. All the occupancies were fixed at nominal composition and kept constant during refinement. Finally, the quality of the fit was assessed from the fit parameters such as R_{wp}, R_p and χ^2.

The morphology of the $NdVO_4$ nanopowders was examined with a Scanning Electron Microscope (SEM) model JEOL JSM 7100F, operating at an accelerating voltage of 10 kV (in secondary electron mode). The samples were first dispersed in ethanol, then few drops of this dispersion were added onto a Si wafer and air dried. The Si wafer was fixed on the SEM sample holder using a carbon tape.

Raman spectroscopy was used for identification and structural characterisation of the $NdVO_4$ nanoparticles. Room temperature Raman spectra were collected in

a 180° backscattering geometry, with a microprobe Raman system type Horiba Jobin-Yvon Lab RAM HR spectrometer equipped with a holographic notch filter and a CCD detector, using a 632.81 nm excitation line of a 25 mW He-Ne laser. The samples were placed and oriented on an Olympus BX 40 microscope equipped with 50× objective and the spectra were recorded in the 50–1000 cm^{-1} range with a resolution of 1 μm. To test the phase purity, the a spot resolution of were recorded on different regions of the sample.

Diffuse reflectance spectroscopy (DRS) measurements were performed to obtain the band gap energies. The DRS spectra were recorded in the 250–800 nm range, with a UV-Vis spectrophotometer (Perkin Elmer, model λ 650S) equipped with a 150 mm integrated sphere and using Spectralon as a reference material. The DRS data were converted to absorbance coefficients according to Kubelka-Munk method where $NdVO_4$ was considered a direct band gap semiconductor.[23] The details of the determination of band gap energies by using the Kubelka-Munk theory are described elsewhere.[24] The photoluminescence (PL) emission spectra were collected with an Edinburgh Instruments Spectrometer (model FLS920) using a steady state 450 W xenon arc lamp. The experimental setup was equipped with a blue-sensitive high speed photomultiplier (Hamamatsu H5773-03 detector) tube. The emission spectra were collected at room temperature, in a 400–700 nm range, using an excitation wavelength of 371 nm (λ_{em} = 524 nm).

Information on the electron relaxation and recombination mechanisms were obtained by monitoring the PL intensity at a specific wavelength as a function of time delay after an exciting laser pulse. The time-resolved PL spectra were recorded at room temperature on a pico-second diode laser EPL 375 with an excitation wavelength of 371 nm, in the time range 0 to 50 ns. The analysis of the fluorescence decays was performed using the F900 analysis software. The measured (convoluted) data was fitted using the "Reconvolution Fit method".[25.] This method fits the sample response to the data over the rising edge, to match the theoretical sample response, $R(t)$. The Reconvolution Fit procedure extracts the raw data (fluorescence decay) and eliminates both the noise and the effects of the exciting light pulse.

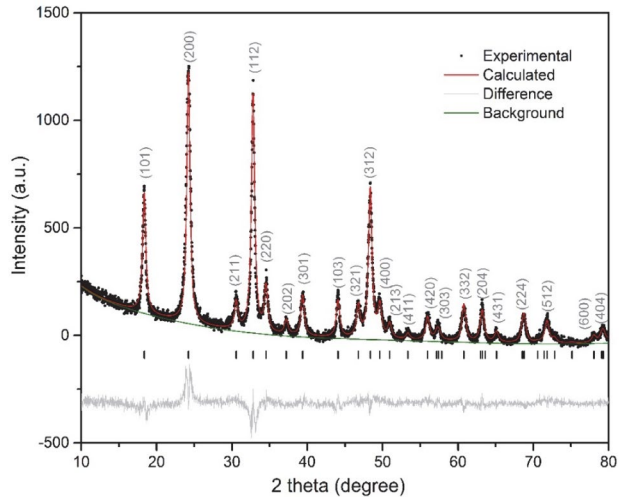

Fig. 2. X-ray powder diffraction pattern of the $NdVO_4$ nanopowder. The black full circles represent raw data and, red solid line is the Rietveld fit, the black vertical bars are the Bragg reflections, while the grey line shown below is the difference between observed and calculated intensity.

3. Results and Discussion

3. 1. X-ray and SEM Studies

Fig. 2 shows the XRPD patterns of the as-obtained $NdVO_4$ sample, which was indexed as a tetragonal $NdVO_4$ phase with the space group $I4_1/amd$ (ICSD code 78077). No impurities were detected. Additionally, the Rietveld refinement indicated that the (112) reflection appears with higher intensity due to the preferred directional growth of the nanoneedles along <112>. The unit cell parameters obtained after the Rietveld refinement are presented in Table 1. The agreement factors were: R_p = 6.59, R_{wp} = 7.78, and χ^2 = 1.26. As it can be seen, the refined cell parameters are in good agreement with the literature reported values.

The particle size and morphology were examined by SEM. From Fig. 3 it can be seen that the $NdVO_4$ particles prepared in this study have a needle-like shape with a length of about 100 nm and a diameter of about 20 nm. A schematic representation showing the $NdVO_4$ nanoneedles grown along <112> is depicted in Fig. 4. The SEM study also showed that the nanoparticles tend to agglomerate leading to formation of larger clusters.

Table 1. The unit cell parameters obtained after Rietveld refinement of the $NdVO_4$ nanoneedles and a comparison with the literature-reported values.

Unit cell parameters Space group: $I4_1/amd$	This study (nanoneedles)	Yuvaraj et al.[26] (27 nm particles)	Fuess et al.[27] (polycrystalline)	Panchal et al.[11] (polycrystalline)
a (Å)	7.3397(6)	7.3571	7.3290	7.334(1)
b (Å)	7.3397(6)	7.3571	7.3290	7.334(1)
c (Å)	6.4128(6)	6.4227	6.4356	6.436(1)
c/a	0.8737(6)	0.8729	0.7878	0.8776(1)
V (Å)	346.332(65)	347.641	345.683	346.177

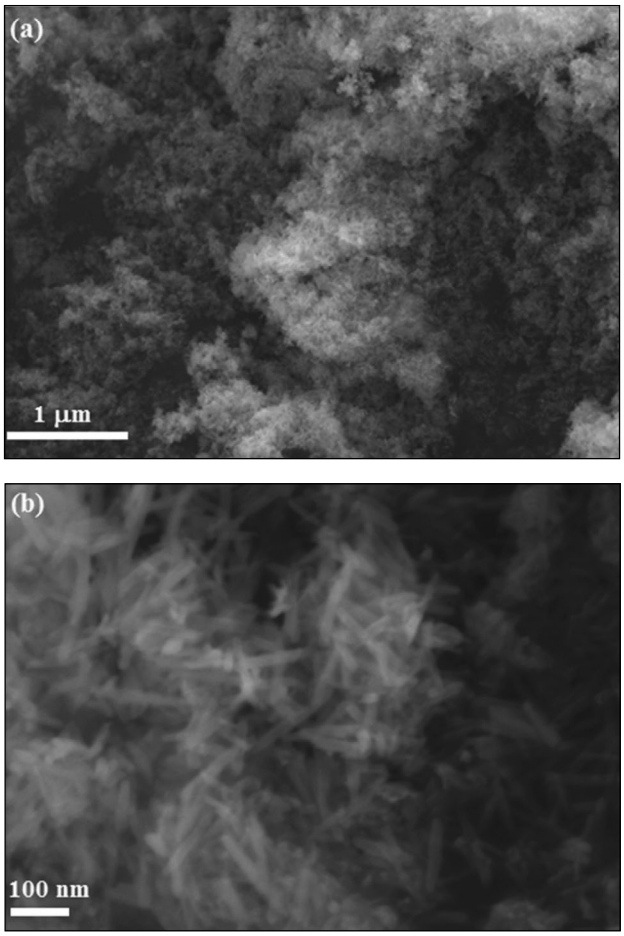

Fig. 3. SEM images of the $NdVO_4$ nanopowders. (a) Low magnification, (b) High magnification.

3. 2. Raman Analysis

Raman analysis was performed on the as-obtained $NdVO_4$ nanopowders to study finer structural details (Fig. 5). As the XRPD analysis already suggested, the $NdVO_4$ synthesised in this study is adopting the zircon-type structure. From a group theory consideration $NdVO_4$ adopting this structure has 12 Raman active modes: $2A_{1g}$, $4B_{1g}$, B_{2g}, and $5E_g$.[28] From these 12 modes, 7 are internal modes associated with vibrations in the VO_4 structural unit ($2A_{1g}$, $2B_{1g}$, $1B_{2g}$, $2E_g$), and 5 are external vibrations ($3E_g$, $2B_{1g}$). So far, the Raman spectra of $NdVO_4$ have been measured on single crystals and polycrystalline samples by several

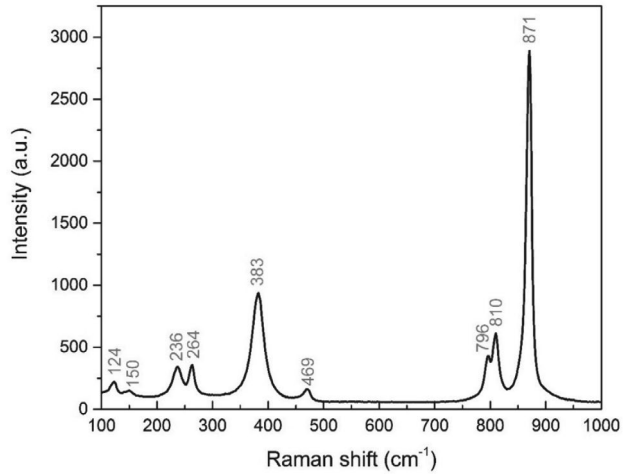

Fig. 5. Raman spectrum of the $NdVO_4$ nanoparticles prepared in this study.

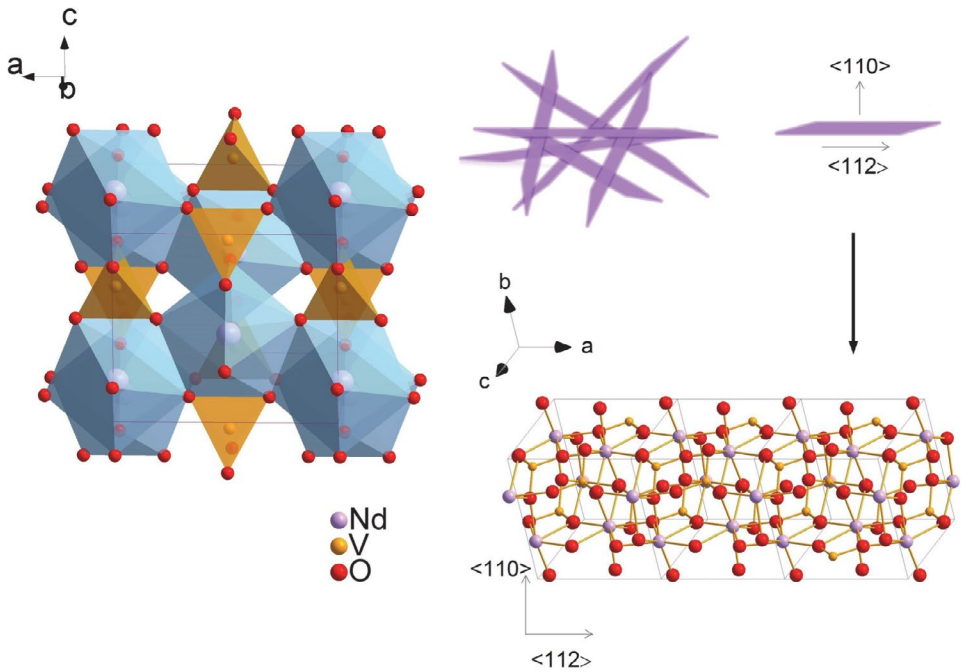

Fig. 4. (a) Crystal structure of $NdVO_4$; (b) Schematic representation of the as-grown $NdVO_4$ nanoneedles; (c) Ball-and-stick model showing a tetragonal $NdVO_4$ nanoneedle grown along <112>.

Table 2. The Raman modes of $NdVO_4$ reported in the literature and the Raman modes observed in this study.

Study	Sample type	Peak position (cm^{-1})											Temp.
This study	Nanoneedles	871	810	796	469	383	–	264	236	150	124	–	297 K
Panchal et al.[11]	Polycrystalline	871	808	794	472	381	373	260	243	151	124	113	297 K
Yuvaraj et al.[26]	Nano rods	876	–	770	–	–	–	–	–	–			297 K
Jandl et al.[29]	Single crystal	873	810	797	472	381	-	259	242	151	122		10 K
Nguyen et al.[28]	Single crystal	871	808	795	472	381	375	260	237	148	123	113	297 K
Antic-Fidancev et al.[30]	Polycrystalline	873	810	797	473	380	378	259	242	151	121	111	4.2 K
		868	805	790	471	380	375	262	235	151	122	112	4.2 K
Santos et al.[31]	Single crystal	871	808	795	472	381	375	260	237	148	123	113	297 K

research groups. A comparison of our results with the literature reports is shown in Table 2.

It can be seen that the observed Raman modes in this study are in good agreement with the literature data. The only modes that were not observed are the modes located at 113, 225, and 373 cm^{-1} (these modes are rarely observed). In the 100–1000 cm^{-1} region, the Raman spectrum of $NdVO_4$ shows 9 modes that are separated in two regions. The high frequency region includes the internal modes in the VO_4 units, whereas the external modes occur at lower frequency and correspond to motions of the Nd–O bonds in the NdO_8 polyhedron. The symmetry annotations were made in accordance with the previous assignments reported in the literature.[10,11,27]

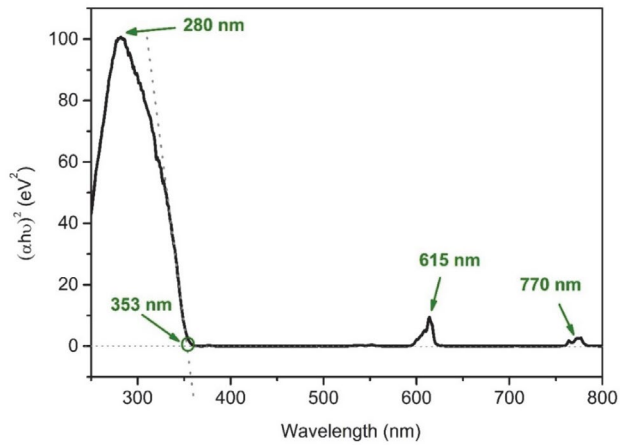

Fig. 6. The UV-Vis diffuse reflectance spectrum of the $NdVO_4$ nanopowder prepared in this study.

3. 3. Optical Studies

Fig. 6 shows the UV-Vis diffuse reflectance spectrum of the $NdVO_4$ nanoneedles prepared in this study.

The light absorption was observed at a wavelength of about 770 nm, followed by another absorption at about 615 nm. A third absorption peak started at about 353 nm, increased sharply and reached a maximum at about 280 nm (associated with the O^{-2}–V^{+5} charge transfer within the VO_4^{3-} group).[32,33] The sharp increase at about 353 nm corresponds to the band gap transition in $NdVO_4$. The additional absorption peaks observed in the UV-Vis spectrum of $NdVO_4$ at about 615 and 770 nm have been described in the literature and they are summarized in Table 3.

From the plot of the absorbance versus the energy (Fig. 7) the band gap of the $NdVO_4$ nanopowders was calculated to be 3.50 eV, which is in the UV region of the electromagnetic spectrum. This value falls well in the range of values reported by other research groups.[8,10]

The electronic structure of zircon-type $NdVO_4$ has also been investigated by Panchal et al.[10] They observed

Table 3. Characteristic peaks observed in the 500–800 nm range in the UV-Vis absorption spectra of $NdVO_4$.

Peak position (nm) (1)	(2)	(3)	Synthesis method and particle size	Study	Comments/ Assignment From $^4I_{9/2}$ to:
–	615	770	Co-precipitation, needles of ~100 nm length and 20 nm diameter	This study	(1) / (2) $^4G_{5/2}$ and (3) $^4F_{7/2}$
–	590	750	Solid-state reactions, ~1 μm.	Dragomir et al.,[24,34] Singh et al.	(1) / (2) $^4G_{5/2}$, (3) $^4F_{7/2}$
532	582	744	Templated sol-gel Nanotubes with the diameter of about 40 nm	Peng et al.[35]	(1) $^4G_{7/2}$ and $^4G_{9/2}$ (2) $^4G_{7/2}$, (3) $^4F_{7/2}$ and $^4S_{3/2}$
538	590	752	Nanowires, 100 nm diameter and 3μm length	Xu et al.[36]	(1) $^2G_{7/2}$, (2) $^4G_{5/2}$, (3) $^4F_{7/2}$
~525	593	753	Hydrothermal, nanorods, length: 400–700 nm.	Wu et al.[37]	(1) $^4G_{7/2}$ and $^4G_{9/2}$ (2) $^4G_{5/2}$, (3) $^4F_{7/2}$

that $NdVO_4$ shows similar band shape with $LuVO_4$ and YVO_4; the upper part of the valence band and the lower part of the conduction band is mainly comprised of the V 3*d* and O 2*p* states, whereas the Nd 6*s* states contribute to a decrease in the band gap due to their hybridization with the antibonding conduction band states.

Under UV excitation (Fig. 8) the $NdVO_4$ nanoneedles show green, yellow, and orange emissions. The $NdVO_4$ spectrum consists of a broad peak centred at about 500 nm with three small shoulders at about 523, 545, and 600 nm. Several researchers have reported the photoluminescence spectra of nanosized $NdVO_4$ (excited with UV light). Wu et al. reported the PL emission spectrum of single crystalline nanorods (of ~200 nm in diameter and 400–700 nm in length).[37] The spectrum shows a strong emission around 490 nm followed by two less intense peaks at ~525 and 550 nm and a triplet at about 600–615 nm.

The $NdVO_4$ nanoneedles prepared in this study show similar peaks. Similar results were also obtained for 1 μm $NdVO_4$ particles prepared by a solid-state method and described by Dragomir et al.[24] Briefly, the emission at about 500 nm can be assigned to the $^4G_{11/2} \rightarrow {}^4I_{11/2}$ transition, whereas the shoulders at ~525, 545, and 600 nm can be attributed to the $^4G_{7/2} \rightarrow {}^4I_{9/2}$, $^4G_{7/2} \rightarrow {}^4I_{9/2}$, and $^4G_{5/2} \rightarrow {}^4I_{9/2}$ transitions, respectively.

Fig. 9 shows the time-resolved photoluminescence spectrum of the $NdVO_4$ nanoneedles excited by a 371 nm laser wavelength and monitored at 524 nm. This decay curve could only be simulated by a third-order exponential function with the three lifetimes: $\tau_1 = 0.16$ ns, $\tau_2 = 1.70$ ns and $\tau_3 = 4.74$ ns. The fitting parameters of the photoluminescence decay curves are presented in Table 4. These results suggest that the PL decay processes were dominated by third order kinetics. To the authors' knowledge, this is the first report on the dynamics of photo-excited carriers in $NdVO_4$.

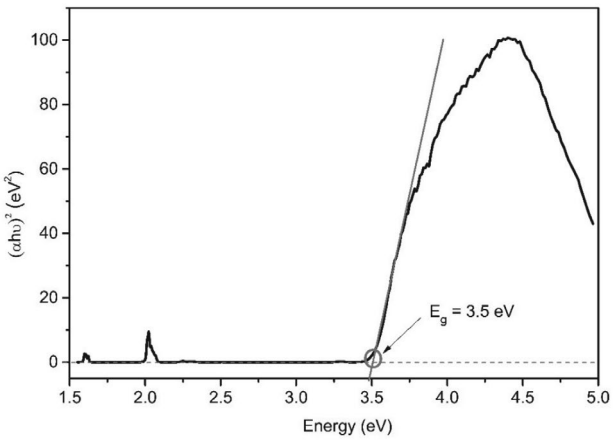

Fig. 7. Optical band gap of $NdVO_4$ nanoparticles.

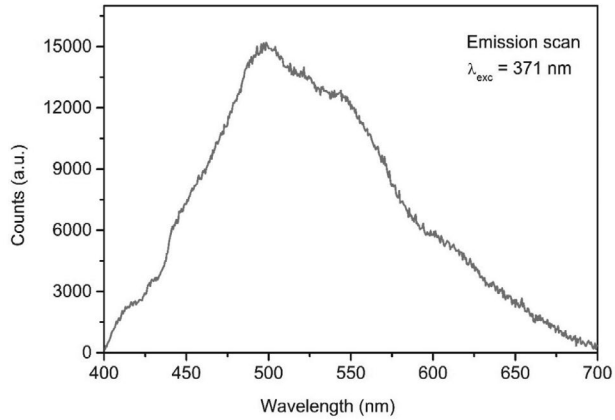

Fig. 8. The emission spectrum of $NdVO_4$ nanoneedles, measured at room temperature.

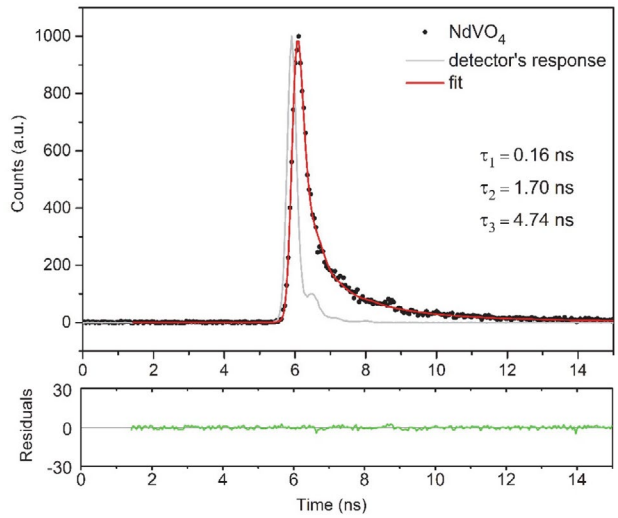

Fig. 9. Photoluminescence lifetime measured on the $NdVO_4$ nanoneedles, $\lambda_{em} = 524$ nm. The black dots represent the time-domain intensity decay. The red line is the fitting curve, while the grey line is the response of the detector. The green line below represents the difference between the fitted curve and the measured data. The goodness of fit, χ^2, is 1.418.

Table 4. Fitting parameters of the photoluminescence decay curves of the $NdVO_4$ nanoneedles ($\lambda_{ex} = 371$ nm, $\lambda_{em} = 524$ nm).

Sample	Lifetime (ns)	Standard deviation (ns)	χ^2	B_1	B_2	B_3
$NdVO_4$ nanoparticles	$\tau_1 = 0.16$ (50.61%)	0.01	1.418	0.35	0.03	0.00
	$\tau_2 = 1.70$ (30.64%)	0.15				
	$\tau_3 = 4.74$ (18.75%)	0.59				

4. Conclusions

A facile room-temperature precipitation method was employed for the synthesis of $NdVO_4$ nanoneedles. This approach utilizes aqueous solutions of $NdCl_3$, Na_3VO_4 and NH_3(aq) as a precipitating agent. The synthesis yielded impurity-free, crystalline $NdVO_4$ nanoneedles with a tetragonal structure, space group $I4_1/amd$. The Rietveld refinement study indicated a preferential growth of the nanoparticles along the <112> direction. The Raman analysis further supported the fact that the nanoparticles are single phase $NdVO_4$ with a zircon-type structure, while SEM analysis showed that the as-synthesised particles have a needle-like morphology with a length of about 100 nm and a width of about 20 nm. The UV-Vis absorption spectrum showed an absorption band located at 353 nm (3.5 eV) which corresponds to the band gap transition. The room-temperature PL spectrum of the $NdVO_4$ nanoneedles shows green, yellow, and orange emissions. The lifetimes of the nanoneedles were monitored for the 524 nm emission and were found to be 4.74 nanoseconds.

In addition to its simplicity, the synthetic method employed in this study also conserves energy since it does not require any thermal treatment. This method could potentially be tailored for the facile preparation of other 1D lanthanide vanadate structures.

5. Acknowledgements

This work was supported by the Slovenian Research Agency under the Young Researchers Programme and the Research Programme P2-0337.

6. References

1. J. A. Baglio, O. J. Sovers. *J. Solid State Chem.* **1971**, *3*, 458–465. **DOI:**10.1016/0022-4596(71)90085-5
2. C.-T. Au, W.-D. Zhang. *Faraday Trans.* **1997**, *93*, 1195–1204. **DOI:**10.1039/a607565g
3. X. Wu, Y. Tao, L. Dong, J. Zhu, Z. Hu. *J. Phys. Chem. B* **2005**, *109*, 11544–11547. **DOI:**10.1021/jp0503922
4. S. Mahapatra, G. Madras, T. N. G. Row. *J. Phys. Chem. C* **2007**, *111*, 6505–6511. **DOI:**10.1021/jp069007e
5. M. Eghbali-Arani, A. Sobani-Nasab, M. Rahimi-Nasrabadi, F. Ahmadi, S. Pourmasoud. *Ultrason. Sonochem.* **2018**, *43*, 120–135. **DOI:**10.1016/j.ultsonch.2017.11.040
6. R. A. Fields, M. Birnbaum, C. L. Fincher. *Appl. Phys. Lett.* **1987**, *51*, 1885–1887. **DOI:**10.1063/1.98500
7. H. Zhang, H. Kong, S. Zhao, J. Jiu et al. *J. Cryst. Growth* **2003**, *256*, 292–297. **DOI:**10.1016/S0022-0248(03)01356-3
8. S. Mahapatra, G. Madras, T. N. G. Row. *Ind. Eng. Chem. Res.* **2007**, *46*, 1013–1017. **DOI:**10.1021/ie060823i
9. A. Di Paola, E. Garcia-Lopez, G. Marci, L. Palmisano. *J. Hazard. Mater.* **2012**, *211–212,* 3–29. **DOI:**10.1016/j.jhazmat.2011.11.050
10. V. Panchal, D. Errandonea, A. Segura, P. Rodriguez-Hernandez, A. Muñoz, S. Lopez-Moreno, M. Bettinelli. *J. Appl. Phys.* **2011**, *110*, 043723. **DOI:**10.1063/1.3626060
11. V. Panchal, D. Erradonea, F. J. Manjon, A. Munoz, P. Rodriguez-Hernandez, S. N. Achary, A. K. Tyagi. *J. Phys. Chem. Solids* **2017**, *100*, 123–133. **DOI:**10.1016/j.jpcs.2016.10.001
12. X. Huang, S. Han, W. Huang, X. Liu. *Chem. Soc. Rev.* **2013**, *42*, 173–201. **DOI:**10.1039/C2CS35288E
13. C. Che Lin, R.-S. Liu. *J. Phys. Chem. Lett.* **2011**, *2*, 1268–1277. **DOI:**10.1021/jz2002452
14. Y. Liu, D. Tu, H. Zhu, X. Chen. *Chem. Soc. Rev*. **2013**, *42*, 6924–6958. **DOI:**10.1039/c3cs60060b
15. C. Yao, Y. Ton. *TrAC, Trends Anal. Chem*. **2012**, *39*, 60–71. **DOI:**10.1016/j.trac.2012.07.007
16. M. Abdesselem, M. Schoeffel, I. Maurin, R. Ramodiharilafy, G. Autret, O. Clément, P.-L. Tharaux, J.-P. Boilot, T. Gacoin, C. Bouzigues, A. Alexandrou. *ACS Nano*, **2014**, *8*, 11126–11137. **DOI:**10.1021/nn504170x
17. S. Mahapatra, S. K. Nayak, G. Madras, T. N. G. Row. *Ind. Eng. Chem. Res.* **2008**, *47*, 6509–6516. **DOI:**10.1021/ie8003094
18. J. Liu, Y. Li. *J. Mater. Chem.* **2007**, *17*, 1797–1803. **DOI:**10.1039/b617959b
19. Z. Xu, C. Li, Z. Hou, C. Peng, J. Lin. *CrystEngComm* **2011**, *13*, 474–482. **DOI:**10.1039/C0CE00161A
20. M. Jang, K. M. Doxsee. *CrystEngComm* **2011**, *13*, 1210–1214. **DOI:**10.1039/C0CE00590H
21. R. Kalai Selvan, A. Gedanken, P. Anilkumar, G. Manikandan, C. J. Karunakaran. *J. Cluster. Sci.* **2009**, *20*, 291–305. **DOI:**10.1007/s10876-008-0229-y
22. R. W. Cheary, A. Coelho. *J. Appl. Crystallogr*. **1992**, *25*, 109–121. **DOI:**10.1107/S0021889891010804
23. P. Kubelka, F. Munk. *Z. Tech. Phys*. **1931**, *12a*, 593–601.
24. M. Dragomir. Ph.D. thesis, **2013**, University of Nova Gorica.
25. Manual of the fluorescence lifetime. Edinburgh Instruments, **2000**, UK.
26. S. Yuvaraj, R. K. Selvan, V. Kumar, I. Perelshtein, A. Gedanken, S. Isakkimuthu, S. Arumugam. *Ultrason. Sonochem.* **2014**, *21*, 599–605. **DOI:**10.1016/j.ultsonch.2013.08.015
27. H. Fuess, A. Kallel. *J. Solid State Chem.* **1972**, *5*, 11–14. **DOI:**10.1016/0022-4596(72)90002-3
28. A.-D. Nguyen, K. M. Murdoch, N. M. Edelstein, L. A. Boatner, M. M. Abraham. *Phys. Rev. B* **1997**, *56*, 7974–7987. **DOI:**10.1103/PhysRevB.56.7974
29. S. Jandl, Y. Lévesque, V. Nekvasil, M. Bettinelli. *Opt. Mater.* **2010**, *32*, 1549–1552. **DOI:**10.1016/j.optmat.2010.07.004
30. E. Antic-Fidancev, J. Holsa, M. Lemaitre-Blaise, P. Porcher. *J. Phys.: Condens. Matter.* **1991**, *3*, 6829–6843. **DOI:**10.1088/0953-8984/3/35/012
31. C. C. Santos, E. N. Silva, A. P. Ayala, I. Guedes, P. S. Pizani, C.-K. Loong, L. A. Boatner. *J. Appl. Phys.* **2007**, *101*, 053511. **DOI:**10.1063/1.2437676
32. Y.-S. Chang, F.-M. Huang, Y.-Y. Tsai, L.-G. Teoh. *J. Lumin*. **2009**, *129*, 1181–1185. **DOI:**10.1016/j.jlumin.2009.05.020

33. N. S. Singh, R. S. Ningthoujam, G. Phaomei, S. D. Singh, A. Vinu, R. K. Vatsa. *Dalton Trans.* **2012**, *41,* 4404–4412. **DOI:**10.1039/c2dt12190e
34. M. Dragomir, I. Arčon, S. Gardonio, M. Valant. *Acta Mater.* **2013**, *61*, 1126–1135. **DOI:**10.1016/j.actamat.2012.10.020
35. X. N. Peng, X. Zhang, L. Yu, L. Zhou. *Mod. Phys. Lett. B* **2009**, *23,* 2647–2653. **DOI:**10.1142/S021798490902076X
36. J. Xu, C. Hu, G. Liu, H. Liu, G. Du, Y. Zhang. *J. Alloys Compd.* **2011**, *509*, 7968–7972. **DOI:**10.1016/j.jallcom.2011.05.051
37. X. Wu, Y. Tao, L. Dong, J. Zhu, Z. Hu. *J. Phys. Chem. B* **2005**, *109*, 11544–11547. **DOI:**10.1021/jp0503922

Povzetek

Tetragonalni $NdVO_4$ v obliki nanoiglic je bil pripravljen s preprosto reakcijo obarjanja pri sobni temperaturi, brez uporabe surfaktantov ali predlog in le iz enostavnih anorganskih soli ($NdCl_3$ in Na_3VO_4). Za karakterizacijo produkta v obliki nanoiglic so bile uporabljene sledeče metode: PXRD, SEM, Ramanska in fotoluminiscenčna spektroskopija ter fotoluminiscenčna dinamika. Dolžina delcev, ki rastejo vzdolž <112> smeri, znaša približno 100 nm, njihov premer pa okoli 20 nm. Opisana metoda, katere prednosti so visok izkoristek, uporaba netoksičnih topil in blagi reakcijski pogoji, je potencialno uporabna tudi za pripravo drugih 1D lantanidnih vanadatov.